Atmospheric Turbulence Statistics and Profile Modeling. Local to DLR Oberpfaffenhofen

Alexander Knoedler, Florian Moll

Atmospheric Turbulence Statistics and Profile Modeling Local to DLR Oberpfaffenhofen

Alexander Knoedler[a] and Florian Moll[a]

[a]German Aerospace Center (DLR), Institute of Communications and Navigation, Wessling, Germany

ABSTRACT

Laser communication (lasercom) is influenced by atmospheric turbulence, a quality measured by the refractive index structure parameter C_n^2. This paper quantifies the degree of improvement to lasercom link budgets afforded by using ground-level measurements of turbulence in vertical turbulence models. Ground-level C_n^2 is measured with an off-the-shelf scintillometer for a path adjacent to DLR's optical ground station (OGS). Measurements are in agreement with literature on turbulence; nighttime C_n^2 is well represented by a log-normal distribution. Comparisons are drawn between profiles by comparing link budget parameter estimates generated by four turbulence profile models: HV-5/7, HV with $C_n^2(h_0)$, and HV and HAP models with $C_n^2(h_0)$ and fitting to downlink experiment data. Vertical turbulence profiles are converted to scintillation index σ_I^2 by way of theory described in the literature on weak and strong turbulence.[1] Normalised root-mean-squared-error is used to establish goodness-of-fit of modeled σ_I^2 to downlink beam parameter measurements . Use of $C_n^2(h_0)$ in a profile model improves upon the fit beyond HV-5/7 by $\approx 8.3\%$. Improvements in the mean expectation from specific fits to satellite downlink experiments improve the NRMSE 30%. However, the variability in margin estimation due to changes in $C_n^2(h_0)$ indicates fitting might not be a consistent improvement over the HV-5/7 model.

This paper describes the setup of the scintillometer, six months of measurements, the use of $C_n^2(h_0)$ measurements in vertical profile models to find the path integrated intensity scintillation index (σ_I^2), and a comparison of modeled-path integrated scintillation index to the scintillation index of downlink ground measurements at DLR's OGS.

Keywords: Refractive index structure parameter, C_n^2, scintillation index, optical communication, downlink, Hufnagel-Valley Profile Modeling, KIODO, optical ground station

1. INTRODUCTION

Measurement of site-specific severity of atmospheric turbulence can improve estimates of free space optical communication (FSOC) system performance. A turbulent atmosphere degrades the quality of a FSOC link; therefore, knowledge of the severity of the turbulence is important for designing a link budget for a FSOC system. The refractive index structure parameter (C_n^2) characterizes the strength of turbulence. To a rough degree, $C_n^2 \approx 10^{-12}$ to 10^{-13} indicates strong turbulence and a $C_n^2 \approx 10^{-15}$ to 10^{-17} indicates weak turbulence.[2] Accurate estimation of C_n^2 over a FSOC link's path yields accurate estimates for link parameters like scintillation index and Fried parameter. The scintillation index (σ_I^2) is used to estimate BER performance and fade statistics for incoherent systems. The accuracy of estimates for C_n^2 are bounded by knowledge of the atmospheric boundary layer, but tractable parametric models of the vertical profile of C_n^2 like the Hufnagel-Valley (HV) or Hufnagel-Andrews-Phillips (HAP) models have been used to make estimations across a path. Those two models in particular rely on accurate knowledge of a ground-reference $C_n^2(h_0)$, a value that is very site-specific and therefore not always well characterized in literature. Chapter 2 will cover how $C_n^2(h_0)$ data was aquired. Chapter 3 will cover preliminary analysis of the scintillation data. Chapter 4 will explain the fit and comparison of profile models. Chapter 5 addresses a preliminary look at the impact of fitted profiles on link budget margin. Chapter 6 covers conclusions and future work.

Further author information: (Send correspondence to F.M.)
A.K.: E-mail: alexander.knoedler@dlr.de
F.M.: E-mail: florian.moll@dlr.de

2. MEASUREMENT SETUP AND DATA AQUISITION

2.1 Theory

A scintillometer is a device that estimates the strength of turbulence in the atmosphere either by measuring temperature and estimating the temperature structure parameter C_T^2 or directly measuring the variation of optical power and backing out the index of refraction structure parameter C_n^2. DLR has installed the latter type of scintillometer (a BLS 900) along a path adjacent to the DLR OGS. The BLS 900 made by Scintec AG is a large-aperture (15 cm), dual-beam instrument that measures C_n^2 . The instrument then derives other atmospheric parameters from C_n^2 such as the scintillation index for a point detector (σ_I^2) and the Fried parameter (r_0). The instrument derives C_n^2 estimations from measurements of the intensity, variation of intensity, and the covariance of the intensity of the two LED beams. The theory behind the instrument is primarily derived from Ref. 3 and Ref. 4. The BLS 900 translates intensity measurements into log-amplitude values,[4] uses the dual-beams to subtract out non-scintillating noise, calculates an initial C_n^2, implements calibrated adjustments for unequal aperture sizes, and adds path-dependent weights and saturation corrections.[3] Values for the scintillation index for a point receiver and estimations of the Fried parameter are then made with the calibrated C_n^2 by equations described in Ref. 4.

2.2 Setup

The BLS 900 receiver is currently configured on top of the roof of Building 103 of DLR's Oberpfaffenhofen site 20 m above ground level (AGL). The transmitter is located approximately 325 m away from the receiver on top of a tower of roughly equal height. The receiver connects to a Scintec weather station that provides measurements of atmospheric pressure, temperature, wind speed, and humidity. These data factor into calculations downstream of C_n^2 and are available in the main data output.

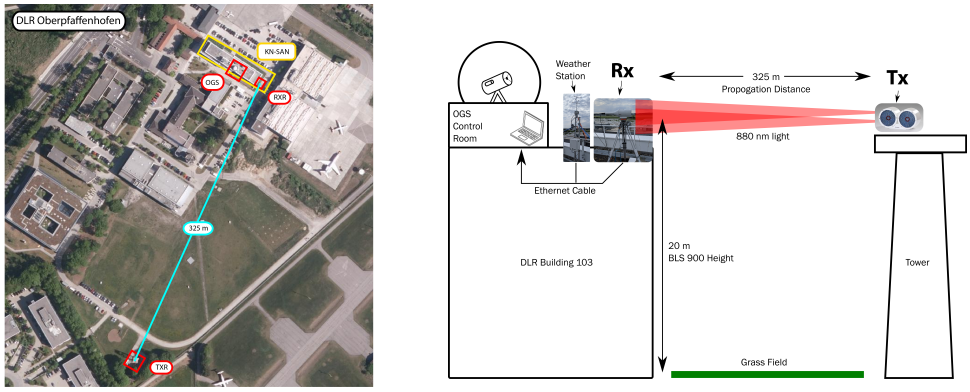

(a) Overhead View of Scintillometer Setup with imagery from Bayern Atlas

(b) Diagram of BLS 900 Setup

Figure 1: Setup of BLS 900 Scintillometer Relative to Optical Ground Station

3. DATA ANALYSIS

3.1 C_n^2 PDFs and Diurnal Cycles

C_n^2 estimations from the scintillometer are in agreement with literature on atmospheric turbulence.[1,2,4] The BLS 900 has been operating almost continuously since late April of 2019 . The data was post-processed and analyzed using MATLAB. Figures 2 and 3 are plots representative of the entire data set up to early September of 2019. The probability density fuctions shown in Figure 2 are simple histograms of C_n^2 in $\log_{10}$ space superimposed with a log-normal distributions derived directly from the mean and variance of the base 10 logarithm of the data. "Day" and "night" are defined by site-specific astronomical sunrise and sunset. FSOC downlinks at DLR occur at night so the nighttime PDF is used for the rest of the paper. The nighttime C_n^2 is on the order of 10^{-15} over the measurement period with a mean value of $\mu = 4.64 \times 10^{-15}$. Standard deviation in linear space is asymetric

but the $\pm\sigma$ range is 1.28×10^{-15} to 1.65×10^{-14}. The nighttime and daytime distributions are similar because of the relationship between astronomical sunrise/set and the heat flux between the air and ground. In qualitative terms, one could distinguish "day" and "night" on the diurnal variation plot by boundaries placed at the valleys near 0500 and 1700 UTC on 2c. However, astronomical day and night are around 0400 and 1900 during this time period. Therefore, the daytime distributions contains the valleys that make the average value more similar to the nighttime distribution.

The diurnal variation plot shown in Figure 2c gives an idea of the mean values and $\pm\sigma$ variation of those mean values. The variance of C_n^2 is occasionally larger than the mean value itself so in some cases the lower bound is not plotable on a log-space chart.

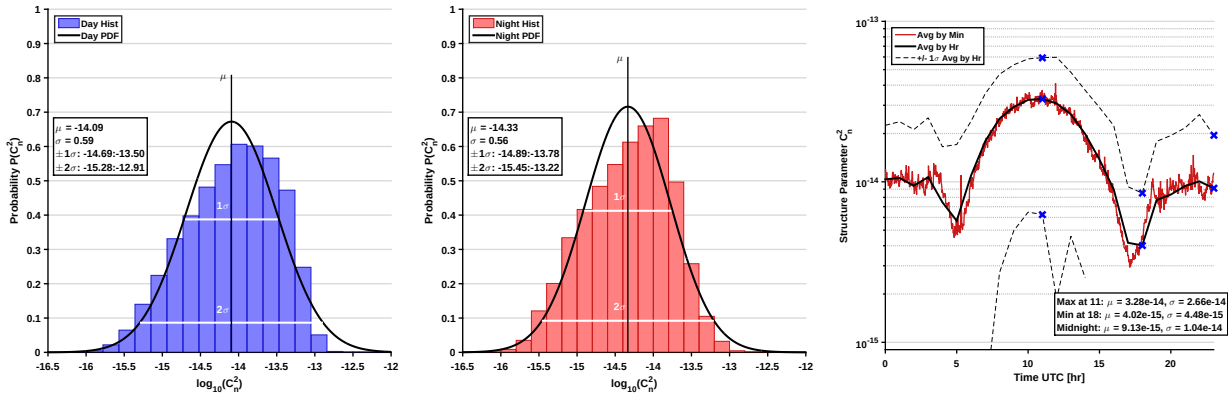

(a) Daytime Log-Normal Fit (b) Nighttime Log-Normal Fit (c) Diurnal C_n^2 Variation

Figure 2: Probability Density Function Estimation for C_n^2

3.2 Data derived from C_n^2

Estimations of the intensity scintillation index and Fried parameter across the scintillometer link are derived from the by-minute measurements of C_n^2. These parameters are plotted across a 24-hour period in Figures 3a and 3b.

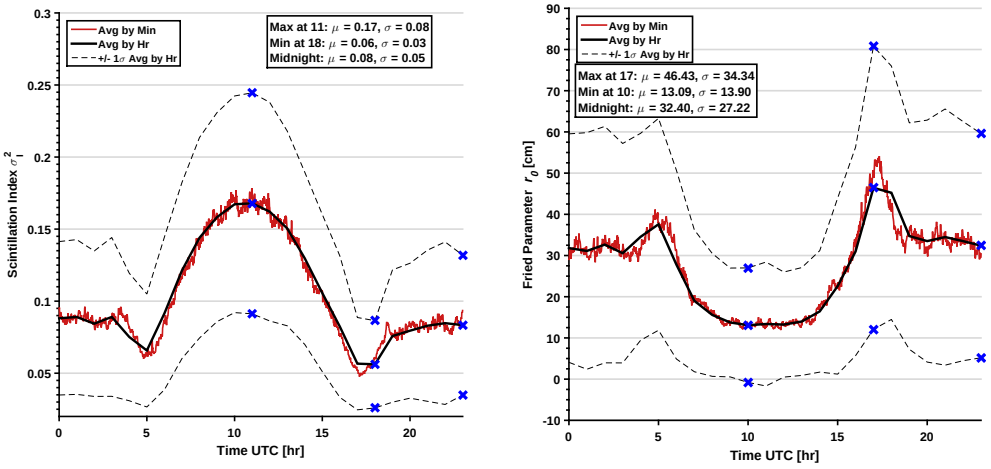

(a) Diurnal σ_I^2 Variation (b) Diurnal r_0 Variation

Figure 3: 24-hr (diurnal) plot of σ_I^2 measurement and Fried Parameter r_0 derived from C_n^2

4. C_N^2 PROFILE MODELING

4.1 Approach

The goal of the profile fitting is to improve profile models for DLR's OGS beyond the textbook Hufnagel Valley 5/7 ($HV_{5/7}$) or a HV model parameterized by a measured ground-level C_n^2. A "best fit" for atmopsheric turbulence profiles was established by fitting profiles to the data from the 2006 KIODO downlink experiment followed by verification of the fitted models against the 2009 KIODO downlink. "DLR performed laser downlinks from the Japanese OICETS [Optical Interorbit Communications Engineering Test Satellite] to the DLR [OGS] in Oberpfaffenhofen near Munich, Germany, in 2006 and 2009... In 2006 ... [eight] trials were performed. In five of them, a link could be established. This campaign was repeated in 2009 ... ten downlinks to the optical ground station at DLR Oberpfaffenhofen were planned, whereas in five signals could be received. Regarding successful data recording, altogether seven of these experiments are used for analysis. ... All measurements took place during spring/summer at nighttime between midnight and two o'clock (UTC)." The OICETS satellite had a downlink beam of 847 nm and the DLR OGS has a 0.4 m cassegrain telescope.[5]

Initial fitting was conducted assuming 847 nm light and the intensity scintillation index, σ_I^2, as the figure of merit. The 2006 experiment has Fried parameter, r_0, data but is r_0 not available in other experiments and is therefore not used. Emphasis on the measurement of intensity scintillation is important, as some downlinks also include the aperture-averaged measurement of the power scintillation index, σ_P^2. Trial KT-07 of Ref. 6. was rejected for uncharacteristically high scintillation following a thunderstorm.

4.2 Initial Fitting of Profiles to KIODO Data

The beam propagation parameter σ_I^2 was compared to actual measurements across the same path during the same time of year (summer). Three profiles were used: HV-Modified, HAP, and HAP-Modified. The Hufnagel-Valley model was modified to represent the OGS height 20 m AGL and the site's height of 600 m above sea level (MSL) in the same way that the HAP altitutde adjustment is made. Modifications to the original equations are in bold, $A = C_n^2(h_0)$, $h \equiv$ altitude above ground, $h_s \equiv$ altitutde of OGS above sea level and $w \equiv$ average wind speed in jetstream.[7]

$$\begin{aligned} C_n^2(h) = {} & 0.00594(w/27)^2(10^{-5} * (h + \mathbf{h_s}))^{10}\exp(-(h + \mathbf{h_s})/1000) \\ & + 2.7 \times 10^{-16}\exp(-(h + \mathbf{h_s})/1500) \\ & + A * \exp(-(h + \mathbf{h_s})/100) \end{aligned} \tag{1}$$

The Hufnagel-Andrews-Phillips model was adjusted from the literature describing the model, Ref. 7. The modification is an addition of an exponential term that supresses the effect of the atmospheric boundary layer (ABL) beyond a kilometer above ground level. This addition is supported by the causal atmospheric mechanisms underpinning vertical profile models that stipulate the heat exchanged at the ground only has an effect to the maximum height of the ABL. In the free atmosphere above the ABL, diurnal variations in the energy transfered to the air from the ground does not affect C_n^2.[8] Without this correction, the $p = 2/3$ power law for nighttime HAP models dramatically overestimates C_n^2 values above 1000 m AGL, even with adjustment to M. The results of the unedited HAP model are not included because of this overestimation but should be noted an acceptable fit is possible using p values valid for the daytime.

$$\begin{aligned} C_n^2(h) = {} & M(0.00594(w/27)^2(10^{-5} * (h + h_s))^{10}\exp(-(h + h_s)/1000) \\ & + 2.7 \times 10^{-16}\exp(-(h + h_s)/1500)) \\ & + A * (h_0/h)^p * \mathbf{exp(-h/1000)} \end{aligned} \tag{2}$$

Each of these models was parameterized across three variables, wind speed $w = 0 : 10 : 80\ m/s$, a constant factor associated with the HAP model $M = 0.1 : 0.1 : 2.1$, and the power law decay of $C_n^2(h_0)$ in the ABL as a function of the hour of day, $p = 2/3$. The power law can be as large as 4/3 but for this analysis, only the

nighttime decay of $p = 2/3$ is considered. The ground reference C_n^2 was held constant at the mean nighttime C_n^2 of our scintillometer data, $\mu = 4.64 \times 10^{-15}$. Each profile had a instrument height $h_0 = 20\ m$ $[AGL]$, OGS altitude $h_s = 600\ m$ $[MSL]$, and atmosphere maximum height $H = 30\ km$ $[AGL]$.

Path integrations of σ_R^2, (weak fluctuation theory) and σ_I^2 (strong fluctuation theory) were evaluated to an altitude of 400 km. These equations can be found in Chapter 12 of Ref. 1 (equations 38 and 40 respectively). The integrated curves were then compared to experimental data and the best parameterization found with the minimization of a goodness-of-fit metric. The fitting metric was the normalized root mean square error of the model to experimental data for an estimation of σ_I^2. The mean of the data was used to normalize RMSE. NRMSE for weak fluctuation theory was only assessed for data where $\sigma_I^2 < 0.5$ and $\zeta < 75$. In the formulation in Eq. 3, $n \equiv$ number of data points, $x_{data} \equiv$ measured values of σ_I^2, $x_{thry} \equiv$ theoretical values of σ_I^2, and $\bar{x}$ indicates the mean.

$$NRMSE_x = \frac{1}{\bar{x}_{data}} \sqrt{\frac{\sum (x_{data} - x_{thry})^2}{n}} \tag{3}$$

In Fig. 4 and 5, Figure 4 from Ref. 6 was recreated and superimposed on the theoretical values for 847 nm light over the same zenith angles (90° - elevation angle). The legend has four theoretical curves. $\text{HVM}_{5/7} \equiv$ the unedited HV-5/7 model for 847 nm light, $\text{HVM}_{\text{h0}} \equiv$ a HV model with $w = 21 m/s$ and $C_n^2(h_0) = 4.64 \times 10^{-15}$, $\text{HVM}_{\text{fit}} \equiv$ a HV model with $C_n^2(h_0) = 4.64 \times 10^{-15}$ but a wind speed fitted to the data, and $\text{HAPM}_{\text{fit}} \equiv$ a HAP model with M and w fitted to data ($p = 2/3$) and $C_n^2(h_0) = 4.64 \times 10^{-15}$.

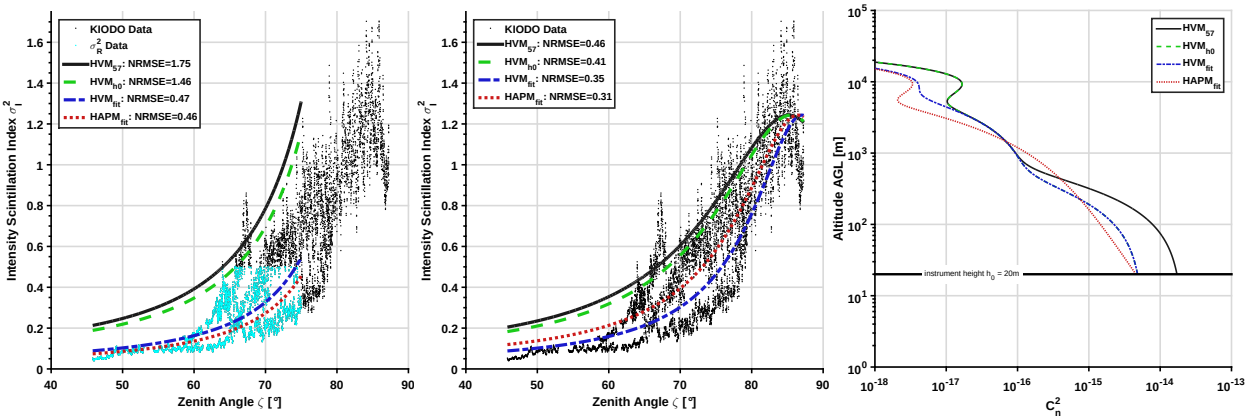

(a) 2006-Weak Theory (b) 2006-Strong Theory (c) C_n^2 vertical profile models

Figure 4: 2006 KIODO measurement campaign data and fits. (a) shows that weak theory requires a fitting process to match the data well. The difference in esitmation in (b) is not as stark but refinement of the vertical profile parameters improves the goodness-of-fit. (c) shows the differences in profiles prior to their inclusion in beam parameters.

In Tables 1 and 2, 24 integrations across a set of zenith angles are provided with their goodness-of-fit metrics. A R^2 is measured from 0 (no correlation) to 1 (perfect correlation). NRMSE of 0 would indicate no error. The first two estimations of each shaded set of rows are un-fitted, i.e., they rely only on data from references or the ground level $C_n^2 = 4.64 \times 10^{-15}$. The final two integrations are the weak and strong theory fits to the adjusted HV and HAP vertical profiles models. Allowing an optimization of NRMSE to drive the parameters of these models reduced the error of the integrations by while maintaining physically reasonable parameters.

4.3 Verfication of Fit within KIODO Data

To ensure the fitting of a profile had not over-fit the parameters to a particular experiement, another goodness-of-fit was performed with the best profiles fit to the 2006 KIODO data against the 2009 KIODO data. The 2006 fits are superimposed on Figure 5. Figure 5a corresponds to Table 3 and Figure 5b corresponds to Table 4. Strong scintillation theory is a better estimation of measured scintillation index as shown in Tables 3 and 4. Inclusion of $C_n^2(h_0)$ does not change the strong scintillation index estimation to a significant degree.

Table 1: Goodness-of-fit metrics for weak scintillation theory, σ_R^2. Correlation (shape) doesn't change as a function of profile but the difference in NRMSE for fitted profiles is clear $C_n^2(h_0) = 4.64 \times 10^{-15}$

Dataset	Model	w	M	$time$	$p(TH)$	$NRMSE(\sigma_R^2)$	$R^2_{\sigma_R^2}$
2006	HVM_{57}	21	-	-	-	1.75	0.30
	HVM_{h0}	21	-	-	-	1.46	0.30
	HVM_{fit}	10	-	-	-	0.47	0.30
	$HAPM_{fit}$	30	0.1	0	2/3	0.46	0.30
2009	HVM_{57}	21	-	-	-	1.37	0.46
	HVM_{h0}	21	-	-	-	1.11	0.46
	HVM_{fit}	10	-	-	-	0.35	0.46
	$HAPM_{fit}$	0	0.9	0	2/3	0.35	0.46
All	HVM_{57}	21	-	-	-	1.57	0.30
	HVM_{h0}	21	-	-	-	1.29	0.30
	HVM_{fit}	10	-	-	-	0.41	0.30
	$HAPM_{fit}$	10	0.5	0	2/3	0.41	0.30

Table 2: Goodness-of-fit metrics for strong scintillation theory, σ_I^2. Each refinement of the profile models improves the NRMSE. The correlation still does not change signficantly, except in the case of 2009 data where fitting by NRMSE actually worsens the correlation. $C_n^2(h_0) = 4.64 \times 10^{-15}$

Dataset	Model	w	M	$time$	$p(TH)$	$NRMSE(\sigma_I^2)$	$R^2_{\sigma_I^2}$
2006	HVM_{57}	21	-	-	-	0.46	0.77
	HVM_{h0}	21	-	-	-	0.41	0.78
	HVM_{fit}	10	-	-	-	0.35	0.76
	$HAPM_{fit}$	50	0.1	0	2/3	0.31	0.78
2009	HVM_{57}	21	-	-	-	0.72	0.63
	HVM_{h0}	21	-	-	-	0.66	0.63
	HVM_{fit}	10	-	-	-	0.49	0.55
	$HAPM_{fit}$	20	0.3	0	2/3	0.49	0.56
All	HVM_{57}	21	-	-	-	0.55	0.68
	HVM_{h0}	21	-	-	-	0.50	0.69
	HVM_{fit}	10	-	-	-	0.40	0.66
	$HAPM_{fit}$	10	0.9	0	2/3	0.38	0.68

Table 3: Comparison of goodness-of-fit metrics for weak scintillation between datasets. Curves fitted to 2006 are compared to 2009 data. The correlations and NRMSEs for the first three profiles are identical to Table 1 because the profile didn't change, even for $\mathrm{HVM_{fit}}$. However, as shown in Row 4 and 8 of Table 1, the profiles are different so the fit to 2009 data is slighly different. $C_n^2(h_0) = 4.64 \times 10^{-15}$

Model	2006 Profiles, 2006 Data		2006 Profiles, 2009 Data	
	$NRMSE_{\sigma_R^2}$	R^2	$NRMSE_{\sigma_R^2}$	R^2
HVM_{57}	1.75	0.30	1.37	0.46
HVM_{h0}	1.46	0.30	1.11	0.46
HVM_{fit}	0.47	0.30	0.35	0.46
$HAPM_{fit}$	0.46	0.30	0.39	0.46

5. APPLICATIONS OF ADJUSTED PROFILES TO LINK BUDGET MARGIN

The use of site-specific parameterizations of tractable turbulence profile models has the potential to improve estimation of atmospheric turbulence effects. While NRMSE relates to how well curves fit to data, more informative

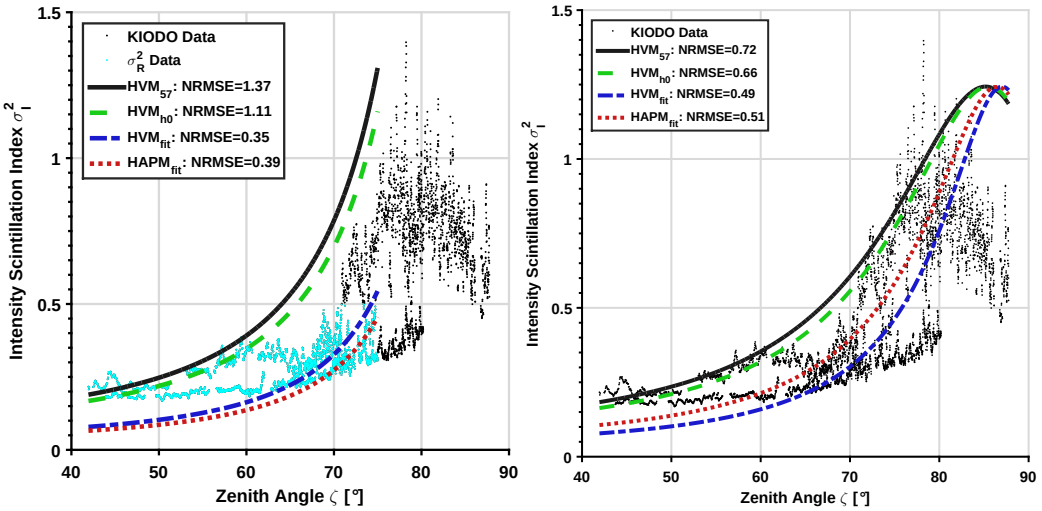

(a) 2009-Weak Theory (b) 2009-Weak Theory

Figure 5: 2009 KIODO Measurement Campaign Data and scintillation models fit to 2006 data. The fit to data is not as good with respect to error or correlation but the fit still improves as a function of profile refinement. This is a good indication that overfitting has not occured

Table 4: Comparison of goodness-of-fit metrics for strong scintilllation between datasets. Curves fitted to 2006 are compared to 2009 data. The correlations and NRMSEs for the first three profiles are identical to Table 2 because the profile didn't change, even for HVM_{fit}. However, as shown in Row 4 and 8 of Table 2, the profiles are different so the fit to 2009 data is slighly different. $C_n^2(h_0) = 4.64 \times 10^{-15}$

Model	2006 Profiles, 2006 Data		2006 Profiles, 2009 Data	
	$NRMSE_{\sigma_I^2}$	R^2	$NRMSE_{\sigma_I^2}$	R^2
HVM_{57}	0.46	0.77	0.72	0.63
HVM_{h0}	0.41	0.78	0.66	0.63
HVM_{fit}	0.35	0.76	0.49	0.55
$HAPM_{fit}$	0.31	0.78	0.51	0.60

metrics of improvment fit directly into a link budget. Conversion to link budget terms followed the approach listed in 9 to establish link margin requirements as a function of scintillation strength and receiver sensitivity.

In Figure 6a, all four profiles are converted from σ_I^2 as a function of ζ to a link budget margin (in dB) as a funciton of ζ for a fade threshold of 10^{-3}. Additionally, the margin of HVM_{h0} and HAPM_{fit} are calculated for the situation where $C_n^2(h_0) = \mu \pm 2\sigma$. $\text{HAPM}_{\text{fit}\pm 2\sigma}$ has a varability beyond that of $\text{HVM}_{\text{fit}\pm 2\sigma}$. This is not a rigorous statistical comparison but does indicate that the use of a fitted HAPM model may experience variablity that makes it unstuitable for link budget estimation.

Figure 6b, the comparison between estimated margins is made explicit. Each margin shown in Figure 6a is subtracted from the textbook HVM_{57} model, showing the difference in mean expected link budget margin. Though there is a distinct difference between the textbook model and the fitted models, the range of variability up to the worst case of the refined models ($\text{HAPM}_{\text{fit}+2\sigma}$ and $\text{HVM}_{\text{fit}+2\sigma}$) contains the textbook HVM_{57} model. A more rigourous approach to link budget modeling, especially at high zenith angles, should be done to establish if ground-level turbulence measurements result in an accurate and significantly different estimation of link budget margin.

6. CONCLUSION

Based on the reasonably good models for intensity scintillation index, there is a difference in the mean margin estimations as a result of fitting to satellite data versus just using ground reference data. Despite an improvement

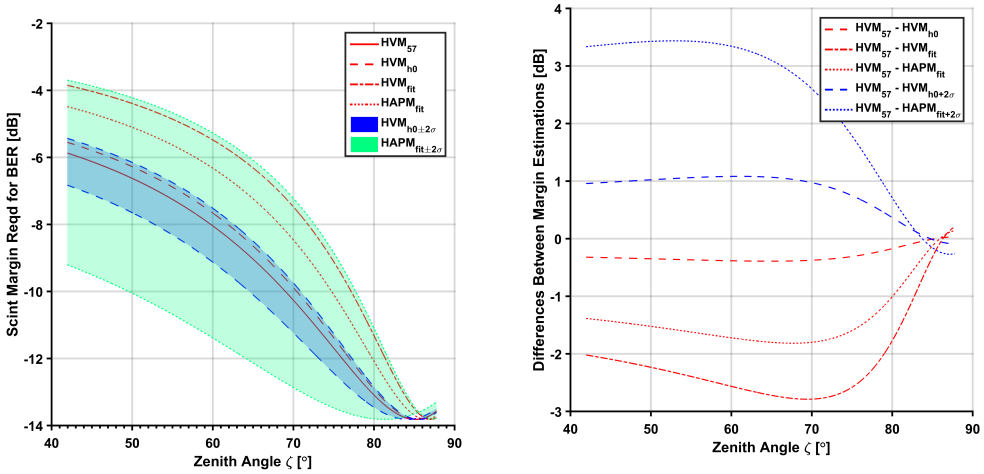

(a) The margin estimated for a threshold of 1e-3 (b) The difference in dB of the margins show in (a).

Figure 6: The link-budget margin in dB required for a set fade probability for each of the vertical profile models (left). A comparison of the sensitivity of margin estimations to variation in ground ref. C_n^2 (right)

in goodness-of-fit, this analysis did not find a significant difference in the margin estimated by the HV-5/7 model and a HV model with accurate ground reference data. The margin derived from fitted profiles relaxes link budget requirements from ground reference profiles. This analysis does not speak to whether or not that will always be the case, fitting could tighten margin requirements relative to ground reference or unedited HV-5/7 estimates.

Further refinement of the link-budget impact of estimated parameters is planned for this set of data, particularly with respect to the sensitivity of the receiver. The impact of variation in the ground reference values of C_n^2 has been given preliminary assesment but more work is required to clarify the variation's impact on link-budget estimations.[10] The impact of scintillometer measured $C_n^2(h_0)$ on parameter estimation should be compared to the impact that Monin–Obukhov estimations of $C_n^2(h_0)$ would have, like the methods described in Ref. [11]. Cloud cover data is available at the DLR-OGS site so there is potential to refine the $C_n^2(h_0)$ distribution to only include measurements during cloud-free nights where links are available.

The introduction of accurate inputs to parameterized vertical turbulence profile improves estimates of beam parameters like scintillation index. However, a link budget designer would need to go as far as fitting their site-specific vertical profile to experimental data to see a significant change in their scintillation margin estimations. That same link budget designer may still want a local scintillometer to calibrate new OGS telescopes or back-plane equipment with the ground reference data.

ACKNOWLEDGMENTS

The authors would like to thank Prof. Kerri Cahoy of MIT STAR Lab for reviewing this manuscript and the MISTI Germany team for facilitating A. Knoedler's work at DLR. Furthermore, we thank Filip Rotrekl for the support in installing and operation of the scintillometer.

REFERENCES

[1] Andrews, L. and Phillips, R., [*Laser Beam Propagation through Random Media*], SPIE Press, Bellingham, Wash., second ed. (2005).

[2] Leclerc, T. T., Phillips, R. L., Andrews, L. C., Wayne, D. T., Sauer, P., and Crabbs, R., "Prediction of the ground-level refractive index structure parameter from the measurement of atmospheric conditions," in [*Atmospheric Propagation VII*], Thomas, L. M. W. and Spillar, E. J., eds., **7685**, 74 – 81, International Society for Optics and Photonics, SPIE (2010).

[3] Wang, T., Ochs, G., and Clifford, S., "A saturation-resistant optical scintillometer to measure c_n^2," *J. Opt. Soc. Am.* **68**, 334–338 (1978).

[4] Lawrence, R. and Strohbehn, J., "A survey of clear-air propagation effects relevant to optical communications," *Proc. Of the IEEE* **58**, 1523–1542 (1970).

[5] Moll, F. and Knapel, M., "Free-space laser communications for satellite downlinks: Measurements of the atmospheric channel," in [*IAC 2011*], *Proceedings of IAC2011* (October 2011).

[6] Moll, F., "Experimental characterization of intensity scintillation in the leo downlink," in [*2015 4th International Workshop on Optical Wireless Communications (IWOW)*], 31–35 (Sep. 2015).

[7] Andrews, L. C., Phillips, R. L., Wayne, D., Leclerc, T., Sauer, P., Crabbs, R., and Kiriazes, J., "Near-ground vertical profile of refractive-index fluctuations," in [*Atmospheric Propagation VI*], Thomas, L. M. W. and Gilbreath, G. C., eds., **7324**, 11 – 22, International Society for Optics and Photonics, SPIE (2009).

[8] Stull, R. B., [*An Introduction to Boundary Layer Meteorology*], Kluwer Academic Publishers, Dordrech The Netherlands, first ed. (1988).

[9] Giggenbach, D. and Henniger, H., "Fading-loss assessment in atmospheric free-space optical communication links with on-off keying," *Optical Engineering* , 046001–1–046001–6 (April 2008).

[10] Giggenbach, D. and Moll, F., "Scintillation loss in optical low earth orbit data downlinks with avalanche photodiode receivers," in [*2017 IEEE International Conference on Space Optical Systems and Applications (ICSOS)*], 115–122 (Nov 2017).

[11] Bendersky, S., Kopeika, N. S., and Blaunstein, N., "Atmospheric optical turbulence over land in middle east coastal environments: prediction modeling and measurements," *Appl. Opt.* **43**, 4070–4079 (Jul 2004).